



Strathprints Institutional Repository

Goetz, Georges and Smith, Richard and Lei, Xin and Galambos, Ludwig and Kamins, Theodore and Mathieson, Keith and Sher, Alexander and Palanker, Daniel (2015) Contrast sensitivity with a subretinal prosthesis and implications for efficient delivery of visual information. Investigative Ophthalmology and Visual Science, 56 (12). pp. 7186-7194. ISSN 0146-0404 , <http://dx.doi.org/10.1167/iovs.15-17566>

This version is available at <http://strathprints.strath.ac.uk/56430/>

Strathprints is designed to allow users to access the research output of the University of Strathclyde. Unless otherwise explicitly stated on the manuscript, Copyright © and Moral Rights for the papers on this site are retained by the individual authors and/or other copyright owners. Please check the manuscript for details of any other licences that may have been applied. You may not engage in further distribution of the material for any profitmaking activities or any commercial gain. You may freely distribute both the url (<http://strathprints.strath.ac.uk/>) and the content of this paper for research or private study, educational, or not-for-profit purposes without prior permission or charge.

Any correspondence concerning this service should be sent to Strathprints administrator: strathprints@strath.ac.uk

1 Contrast sensitivity with a subretinal prosthesis and implications 2 for efficient delivery of visual information

3 Georges Goetz^{1,2}, Richard Smith⁴, Xin Lei², Ludwig Galambos², Theodore Kamins²,
4 Keith Mathieson⁵, Alexander Sher^{† 4}, Daniel Palanker^{† 1,3}

5
6 ¹Hansen Experimental Physics Laboratory, ²Department of Electrical Engineering,,³Department of
7 Ophthalmology Stanford, CA 94305, USA.

8 ⁴Santa Cruz Institute for Particle Physics, University of California Santa Cruz, Santa Cruz, CA 95064,
9 USA.

10 ⁵Institute of Photonics, University of Strathclyde, Glasgow, Scotland G4 0NW, UK.

11 **Word count:** Abstract 316 words, text 4556 words.

12 **Purpose:** To evaluate the contrast sensitivity of a degenerate retina stimulated by a photovoltaic
13 subretinal prosthesis, and assess the impact of low contrast sensitivity on transmission of visual
14 information.

15 **Methods:** We measure *ex-vivo* the full-field contrast sensitivity of healthy rat retina stimulated with
16 white light, and the contrast sensitivity of degenerate rat retina stimulated with a subretinal
17 prosthesis at frequencies exceeding flicker fusion (>20Hz). Effects of eye movements on retinal
18 ganglion cell (RGC) activity are simulated using a linear-nonlinear model of the retina.

19 **Results:** RGCs adapt to high frequency stimulation of constant intensity, and respond transiently to
20 changes in illumination of the implant, exhibiting responses to ON-sets, OFF-sets, and both ON- and
21 OFF-sets of light. The percentage of cells with an OFF response decreases with progression of the
22 degeneration, indicating that OFF responses are likely mediated by photoreceptors. Prosthetic vision
23 exhibits reduced contrast sensitivity and dynamic range, with 65% contrast changes required to
24 elicit responses, as compared to the 3% (OFF) to 7% (ON) changes with visible light. The maximum
25 number of action potentials elicited with prosthetic stimulation is at most half of its natural
26 counterpart for the ON pathway. Our model predicts that for most visual scenes, contrast sensitivity
27 of prosthetic vision is insufficient for triggering RGC activity by fixational eye movements.

28 **Conclusions:** Contrast sensitivity of prosthetic vision is 10 times lower than normal, and dynamic
29 range is two times below natural. Low contrast sensitivity and lack of OFF responses hamper
30 delivery of visual information via a subretinal prosthesis.

31 **Financial disclosure:** D.P.'s patents related to retinal prostheses are owned by Stanford University
32 and licensed to Pixium Vision. D.P. is a consultant for Pixium Vision.

33 **Funding sources:** Funding was provided by the National Institutes of Health (grant R01-EY-018608,
34 D.P.), the Department of Defense (grant W81XWH-15-1-0009, D.P.) and the Stanford Spectrum fund
35 (D.P.). A.S. was supported by BWF CASI and Pew Charitable Trusts Scholarship in the Biomedical
36 Sciences. K.M. was supported by an SU2P fellowship as part of an RCUK Science Bridges award.

1 Introduction

2 Retinal degenerative diseases such as age-related macular degeneration and retinitis pigmentosa are
3 among the most common causes of untreatable blindness in the developed world¹. In these diseases,
4 the image-capturing photoreceptors degrade, while cells in the image-processing layers of the retina
5 can remain relatively intact²⁻⁴, albeit with sometimes extensive rewiring⁵, allowing for the possibility
6 of sight restoration via electrical stimulation of these surviving neurons. The epiretinal approach to
7 retinal prostheses involves direct stimulation of the retinal ganglion cells (RGCs)⁶, while the
8 subretinal approach primarily targets the bipolar cell layer⁷. With both approaches, prosthetic
9 systems currently approved for clinical use involve cumbersome implants wired to extraocular
10 power supplies, necessitating complex surgeries.

11 To address this issue, we developed a modular, easy-to-implant photovoltaic subretinal prosthesis
12 system in which power and visual information are delivered directly to each pixel by light projected
13 from video goggles⁷⁻⁹. The light is pulsed to provide bi-phasic charge-balanced stimulation¹⁰ required
14 for electrochemical biocompatibility. Use of a near-infrared wavelength (880-915nm) allows
15 avoiding both photophobic and phototoxic effects of bright illumination. Processing of the visual
16 signal between the camera and the head-mounted display can be individually tailored to each
17 patient.

18 A recent study has demonstrated both *ex-* and *in-vivo* that the resolution of this implant corresponds
19 to its 65 μ m pixel pitch¹¹. However, it did not address the problem of delivering multiple gray levels
20 to the implant. In the present paper, we therefore consider retinal responses to changes in luminance
21 over the array, comparing the full-field contrast sensitivity of prosthetic stimulation of degenerate
22 rat retina with that of normal vision in healthy retinas. Since the contrast sensitivity with subretinal
23 electrical stimulation was found to be much lower than normal, we explore through simulations the
24 implications of this finding for efficient delivery of visual information.

25 In the case of normal vision, the statistics of natural scenes, fixational eye movements (FEMs) and the
26 contrast sensitivity of retinal ganglion cells are all well-tuned to each other and enable efficient

1 encoding of the visual signal^{12, 13}. We show that the reduced contrast sensitivity and lack of OFF
2 responses in prosthetic vision introduces a mismatch in this encoding machinery. We predict that the
3 majority of FEMs cannot trigger RGC responses with such low contrast sensitivity, which could
4 explain image fading at high stimulation frequencies in patients with subretinal prostheses¹⁴.

5 **Methods**

6 ***Implant fabrication***

7 We manufactured photovoltaic arrays on silicon-on-insulator wafers using a six-mask lithographic
8 process, as described previously¹⁵. To produce anodic-first pulses of electric current, we reversed the
9 n-doped and p-doped regions in the diodes compared to the previous description. Photovoltaic
10 arrays consisted of 70 or 140 μm pixels, separated by 5 μm trenches. Each pixel contained two
11 photodiodes connected in series between the active and return electrodes arranged in a hexagonal
12 array. A resistance between the active and return electrodes helps discharge them between the light
13 pulses, thus achieving charge balance.

14 ***Electrophysiological recordings***

15 We obtained rats with retinal degeneration (P90-140, $n = 5$; p300-400, $n = 2$) from a Royal College of
16 Surgeons (RCS) colony maintained at the Stanford Animal facility. Female Long-Evans adult WT rats
17 ($n = 4$) were purchased from Charles River (Wilmington, MA, USA). All animals were housed in a 12-h
18 light/12-h dark cycle with food and water ad libitum. We conducted all experimental procedures in
19 accordance with the Stanford University and University of California Santa Cruz institutional
20 guidelines, and conformed to the guidelines of the Association for Research in Vision and
21 Ophthalmology (ARVO) Statement for the Use of Animals in Ophthalmic and Vision research.

22 The animals were euthanized (390 mg/ml pentobarbital sodium, 50 mg/ml phenytoin sodium)
23 before one eye was enucleated. We isolated a small piece of retina ($\sim 3 \times 3 \text{mm}$) and placed it on the
24 512-electrode recording array¹⁶ ganglion cell side down. We recorded from one piece of retina per
25 animal. The photovoltaic array was then placed on top of the retina, simulating a subretinal

1 placement *in-vivo*⁷. We ensured good contact between the retina and the stimulating and recording
2 arrays by carefully pressing down on the implant with a plastic mesh. We perfused the retina with
3 Ames solution (Sigma-Aldrich) saturated in oxygen and kept at 27°C. Voltage waveforms were
4 sampled and recorded at 20kHz on each of the 512 electrodes of the recording array¹⁶.

5 ***Visual stimulation***

6 For evaluation of prosthesis-mediated vision, we activated the photovoltaic array using a near-
7 infrared (NIR) projection system, which consisted of a polarization-scrambled array of NIR (880 nm)
8 laser diodes coupled into a 400 μm multimode fiber (Dilas M1F4S22-880.3-30C-SS2.1). We
9 collimated the laser beam at the output of the fiber and used a 2° divergence microlens array diffuser
10 to improve beam homogeneity. The beam was projected onto the implant via the camera port of an
11 inverted microscope (Olympus IX-71, 5x objective). We controlled the timing, width and amplitude of
12 the light using a National Instruments USB-6353 data acquisition card and custom software.

13 For evaluation of the natural responses to visible light, we projected the optically minified image of a
14 15" CRT screen (model Sony CPD-E100) on the photoreceptor layer of a healthy retina through the
15 camera port of the inverted microscope. We modulated the light intensity over the full field using
16 randomized light pulses drawn so as to keep a mean luminance level corresponding to 0.5 of the
17 maximum brightness over the duration of the stimulus. The light flux at the 0.5 gray background level
18 was equivalent to 19,000 photons/ $\mu\text{m}^2/\text{s}$ produced by a monochromatic source of wavelength 515
19 nm. Each intensity step lasted 0.5 second before a 0.5 second-long step to the following intensity (Fig.
20 1A). We kept intensities between the $0.5-0.48 = 0.02$ and $0.5+0.48 = 0.98$ levels, which correspond to
21 the limits of the range of intensities over which we are able to modulate the pixels intensity on the
22 CRT linearly. We used $n = 100$ trials for each intensity value in order to detect deviations from the
23 spontaneous firing rate that are half its standard deviation or larger, with a P value of 0.01 and a
24 statistical power of 0.8, for which a minimum of $n = 94$ trials is required¹⁷.

25 For evaluation of responses to prosthetic stimulation, we used a carrier waveform consisting of 20
26 Hz, 4 ms pulses of NIR light. We modulated the envelope of the carrier waveform using a square wave
27 consisting of a 0.5 second-long maximum value of 2.5 mW/ mm^2 (140 μm pixels) or 5mW/ mm^2 (70 μm

1 pixels) followed by a 0.5 second-long OFF value randomly selected from a pre-determined list of
2 values between 0 and the maximum intensity (Fig. 1B). We used $n = 150$ trials for each intensity
3 value, in order to maintain adequate statistical power with increased noise levels due to electrical
4 stimulation.

5 In addition to full-field light intensity steps, we stimulated the WT retinas with a spatio-temporal
6 white noise, which allowed us to calculate spike triggered average (STA) response of the detected
7 RGCs¹⁸. Time dependence of the calculated STAs was used to classify cells into ON-center and OFF-
8 center types¹⁹. The spatiotemporal monochromatic white noise stimulus consisted of 100 x 60
9 square pixels with each pixel 70 μm on a side, refreshed every 33.33 ms. We randomly set the
10 relative intensity level for each pixel in each frame above or below the 0.5 mean background level at
11 0.5 ± 0.48 . The corresponding contrast, $(I_{\text{max}} - I_{\text{min}})/(I_{\text{max}} + I_{\text{min}})$, was therefore 96%, where I_{max} and
12 I_{min} are the maximum and minimum intensities, respectively.

13 ***Data analysis***

14 For prosthetic stimulation data, we initially subtracted stimulation artifacts from the raw voltage
15 traces recorded on the electrode array and subsequently analyzed the data using custom-written
16 software¹⁶. We estimated electrical stimulation artifacts by averaging their shape over many (100+)
17 trials. The average artifact shape was subsequently aligned to the raw recordings and pointwise
18 subtracted from them. This method was sufficient for removal of the artifact immediately following
19 the pulse, but often insufficient for the artifact removal during the light pulse, therefore we blanked
20 this phase during processing of the recordings (Fig 1C-D). As a consequence, all possible direct
21 stimulation of the RGCs (latency $\leq 1\text{ms}$ ²⁰) was ignored in our analysis.

22 We performed action potential detection by thresholding the artifact-removed data. All action
23 potential waveforms were aligned to the time of maximum deflection from baseline, and we
24 performed dimensionality reduction on the waveforms by principal component analysis, prior to
25 expectation-maximization clustering^{16, 21}. For each putative neuron, we calculated the
26 electrophysiological image (EI) of the neuron, i.e. the average voltage waveform recorded on the
27 whole multielectrode array when the neuron produced an action potential²²⁻²⁴. We discarded

1 neurons exhibiting abnormal EIs from the analysis, as well as neurons for which violations of the
 2 refractory period occurred within the action potential train. Finally, we removed neurons with the
 3 same EI from the analysis, as they correspond to redundant detections of a single neuron over
 4 multiple electrodes, and only the putative neuron with the largest action potential count was kept.
 5 The neuron selection process is described in more details in the literature^{7, 11}.

6 For each contrast step, we constructed peristimulus time histograms (PSTHs) by binning action
 7 potentials over 5 ms periods and averaging over 100 (visible) or 150 (prosthesis) trials. We used the
 8 Michelson definition for contrast $(I_{\text{post}} - I_{\text{pre}})/(I_{\text{post}} + I_{\text{pre}})$, where I_{pre} is the luminance (or peak
 9 intensity for prosthetic stimulation) pre contrast step and I_{post} is the luminance post contrast step.
 10 We defined the steady-state retinal activity as the firing rate over the 300-500 ms period post-
 11 stimulus. For visible light stimulation, we compared the steady-state activity to the activity in the 50-
 12 150 ms following each contrast step. The amplitude of the response was quantified as the positive
 13 variation from steady-state activity in number of action potentials. For prosthetic stimulation, latency
 14 of the elicited action potentials was shorter than for visual stimulation⁷, likely because electrical
 15 stimulation bypasses the slow phototransduction cascade. Therefore, steady-state activity was
 16 compared to the activity in the 5-100 ms following each contrast step. All neurons that did not
 17 respond to at least one value of contrast change with an average of 0.5 action potential elicited per
 18 trial were considered non-responsive and were discarded from the analysis. We included in the
 19 analysis the experimental preparations in which at least 10 RGCs underneath the implant responded
 20 to 100% contrast steps over the full-field.

21 For each neuron, we plotted the number of elicited action potentials vs. amplitude of the contrast
 22 step and fitted the resulting curves with two generalized sigmoid functions, one for the OFF
 23 component of the response and the other for the ON component, such that:

$$\begin{cases} r = f(\log -c, \tau_l, \mu_l, \sigma_l, \rho_l) & \text{if } c < 0 \\ r = 0 & \text{if } c = 0 \\ r = f(\log c, \tau_r, \mu_r, \sigma_r, \rho_r) & \text{if } c > 0 \end{cases}$$

24 where $f(x, \tau, \mu, \sigma, \rho) = \tau \left(1 + e^{-(x-\mu)/\sigma}\right)^{-\rho}$, c is the contrast and r the response of the neuron.

1 We defined the stimulation threshold as a 50% probability of eliciting an action potential, as
2 estimated from the generalized sigmoid fit. We classified neurons that responded primarily to
3 luminance increments with prosthetic stimulation as electrical ON cells, neurons that responded
4 primarily to luminance decrements as electrical OFF cells and neurons that responded to both
5 luminance increments and decrements as eON-OFF cells. The classification was based on three
6 ranges of the ratio of $\max(\text{ON response})/\max(\text{OFF response})$: $<1/3$ – eOFF, $[1/3, 3]$ – eON-OFF and
7 >3 – eON.

8 **Results**

9 ***RGC responses to contrast steps***

10 In normal retina, visual information is transduced by the photoreceptors, further processed in the
11 inner nuclear layer and ultimately transmitted to the RGCs, which relay it to the brain. The receptive
12 fields of different RGC types form complementary mosaics over the retinal surface^{19, 25-28}. Very
13 generally, RGCs respond to changes in luminance by generating action potentials in response to light
14 increments (ON- cells), or decrements (OFF- cells), or both increments and decrements in
15 illumination (ON-OFF cells)²⁹. In this study we did not classify RGCs by their direction-of-motion or
16 object-motion selectivity^{30, 31}.

17 To measure contrast sensitivity of the healthy (wild-type, Long Evans, WT) rat retina, we projected
18 full-field visible light steps of varying amplitude on the photoreceptor layer. We projected similar
19 patterns on a photovoltaic implant pressed on the photoreceptor side of WT and degenerate (Royal
20 College of Surgeons, RCS) rat retina using high frequency near infrared (NIR) illumination (Methods
21 and Fig. 1). We recorded from $n = 360$ neurons for visible light stimulation of the WT retina, $n = 75$
22 neurons for prosthetic stimulation of the WT retina, $n = 91$ neurons for prosthetic stimulation of the
23 P90-140 RCS retina using $70 \mu\text{m}$ pixel size implants, $n = 65$ neurons for prosthetic stimulation of the
24 P90-140 RCS retina using $140 \mu\text{m}$ pixel size implants and $n = 28$ neurons for prosthetic stimulation of
25 the P300-400 RCS retina using $140 \mu\text{m}$ pixel size implants. Responses to both visible light stimulation
26 and near-infrared stimulation could be classified as ON, OFF or ON-OFF (Methods and Fig. 2). We will

1 denote visible light responses as vON (Fig. 2B), vON-OFF (Fig. 2C) and vOFF (Fig. 2D) in the rest of
2 the text in order to distinguish them from their prosthetic counterparts, electrical eON (Fig. 2E), eON-
3 OFF (Fig. 2F) and rare, weak eOFF (Fig. 2G, $n = 9/75$ neurons for WT retina and $n = 2/184$ neurons
4 for RCS retina).

5 Responses to prosthetic stimulation exhibited shorter latencies than responses to visible light
6 (typical latency of 5-100ms following the contrast step, as compared to latencies of 50-150ms for
7 visible light stimulation), likely because prosthetic stimulation bypasses the slow phototransduction
8 cascade⁷. The ratio of prosthetic stimulation thresholds between ON-center and OFF-RGCs in WT
9 retinas was 1.24 ± 0.31 (mean \pm SEM), not substantially different between the two cell classes.

10 The proportion of eON, eOFF and eON-OFF responses varied significantly between healthy and
11 degenerate animals as well as between RCS animals at different stages of degeneration. For WT
12 animals, purely eON responses accounted for 32% of the responsive neurons we recorded from. For
13 p90-140 RCS animals, this fraction went up to 68% and for p300-400 animals, 89% of the responses
14 to electrical stimulation did not have any OFF component anymore (Table 1). In the WT retina,
15 among OFF-center RGCs (identified from a binary white noise stimulus, Methods), 56% responded as
16 purely eON, while 22% responded as eON-OFF and 22% as eOFF cells. ON-center RGCs responded
17 primarily (83%) as eON-OFF cells, with another 14% responding as eON cells and the other 3%
18 responding as eOFF cells (Table 2).

19 The reduction in the fraction of eOFF responses with time indicates photoreceptor involvement in
20 their generation. Histological analysis of the WT and RCS retina (Fig. 3) reveals that while the
21 photoreceptor outer segments have degenerated by P90 in the RCS retina, a significant fraction of the
22 photoreceptor somas remain, which could account for the remaining eOFF responses at P90. At P400,
23 the photoreceptor somas are virtually all gone, as is the eOFF component of the response.

24 ***Contrast sensitivity of the retinal response to prosthetic stimulation***

25 Plotting the mean population response to contrast steps (Fig. 4) reveals two striking features of
26 prosthetic vision, compared to natural light responses: (a) dynamic range of the responses is

1 considerably reduced and (b) very large contrast steps are required to elicit reliable responses in the
2 RGCs.

3 We defined stimulation thresholds as a 50% probability of eliciting an action potential^{7, 11, 32, 33}
4 (Methods). For visible light stimulation, the mean stimulation threshold was 7% positive contrast for
5 vON cells, and 3% negative contrast for vOFF cells. When stimulating p90-140 and p300-400 RCS
6 retina with either 70 μ m or 140 μ m pixel size implants, stimulation threshold was measured to be
7 between 56% (p300-400 RCS retina, 140 μ m pixels) and 70% (p90-140 RCS retina, 140 μ m pixels)
8 contrast. Maximum amplitude of the response was on average 3.6 action potentials per contrast step
9 for vON responses of the WT retina and 7.2 action potentials per contrast step for vOFF responses
10 (Fig. 4A). Amplitude of the response was significantly reduced with prosthetic stimulation of
11 degenerate tissue, with only 1.2 action potentials per contrast step for stimulation of p90-140 RCS, in
12 the eON response. Since eOFF and eON-OFF responses in degenerate tissue largely disappear at the
13 later phases of degeneration, we will ignore the few neurons that were detected as eOFF or eON-OFF
14 in RCS tissue in further analysis.

15 We did not observe a significant change in contrast sensitivity thresholds or amplitude of the
16 response of RCS retina to prosthetic stimulation with age (Fig. 4C, D; $P = 0.21$ and $P = 0.27$ for a
17 change in contrast sensitivity and amplitude, respectively, two-sample KS test), or with the size of the
18 stimulating pixel (Fig. 4B, C; $P = 0.66$, two-sample KS test): 1.2 action potentials were elicited per
19 contrast step in p90-140 RCS retina with both 70 and 140 μ m pixels, and 1.5 action potentials elicited
20 in p300-400 RCS retina with 140 μ m pixels. This result suggests that while pixel size affects
21 stimulation thresholds^{8, 34}, it might not influence significantly the contrast sensitivity once the
22 irradiance is modulated around a constant adaptation level far above stimulation threshold.

23 ***Delivering visual information with a subretinal prosthesis***

24 Visual perception of brightness is determined primarily by local spatio-temporal contrast of the
25 visual stimulus^{13, 35, 36}. During visual fixation of a static scene, the retina locally adapts to the average
26 luminance over the course of a few hundred milliseconds³⁷. RGCs then respond to local changes in
27 contrast triggered by ocular movements such as microsaccades, drift and ocular tremor. It has been

1 hypothesized that ocular movements prevent perceptual fading by continuously stimulating neurons
2 that respond transiently to stimuli³⁸ and contribute to encoding of visual scenes¹³.

3 Fixational eye movements (FEMs) transform static spatial modulation in luminance in images into
4 temporal modulation of luminance on the retina. Recent studies^{12, 13} have shown that the statistical
5 properties of FEMs are well tuned to the statistics of natural scenes and perform whitening of spatial
6 frequencies below 30 cycles per degree – the resolution limit of a typical human eye. Contrast
7 sensitivities of RGCs are, in turn, well adapted to the resulting spatio-temporal patterns of light on
8 the retina, producing robust RGC responses. Prosthetic vision exhibits much lower full-field contrast
9 sensitivity and a lack of OFF responses, which is likely to disrupt these finely tuned fixational
10 mechanisms.

11 To illustrate the effect of reduced contrast sensitivity on the ability of the retina to encode visual
12 information, we considered a 1-dimensional step in intensity (Figure 5A, top panel) and estimated
13 the contrast between the light pattern and the static component of the retinal image caused by visual
14 fixation¹². This static component, the local average luminance, was obtained by convolution of the
15 light step with a blurring kernel defined by the distribution of eye movements (Figure 5A, middle
16 panel). The underlying assumption is that the amplitude of FEMs determines the spatial scale over
17 which the average luminance on the retina is determined. Amplitude of the blurring kernel decreases
18 proportionally to one minus the cumulative distribution function of microsaccades³⁹ and the
19 probability distribution function of microsaccade amplitude is modeled as a gamma distribution,
20 with shape parameter 2 and scale parameter 0.15° .

21 The maximum positive contrast between a step pattern and its local average luminance is $1/3$,
22 independently of the width of the blurring kernel (Figure 5A, lower panel), much lower than the
23 contrast stimulation threshold with prosthetic vision. Large lateral displacements of the pattern – on
24 the order of the size of the blurring kernel – are required to cause a 60% change in local contrast. In
25 other words, only large and rare microsaccadic eye movements can trigger a sufficient change in
26 luminance for eliciting retinal activity.

1 To guarantee that any displacement of the image will trigger an ON response in a system with
2 contrast sensitivity c , a binary image should be at least locally x -sparse, where $x = (1-c)/(1+c)$ on the
3 spatial scale of the luminance averaging. In the 1-dimensional case, a thin line meets this criterion
4 (Figure 5B), so any small displacement of the pattern can introduce sufficient changes in the local
5 contrast to trigger a response. For prosthetic vision with contrast sensitivity thresholds around 60%,
6 this criterion means that binary images should be at least locally 25% sparse to efficiently deliver
7 visual information. The more images deviate from this criterion, the less retinal activity will be
8 elicited by the temporal changes in luminance produced by FEMs.

9 Most static visual scenes in general, and natural scenes in particular, fail to meet such a local sparsity
10 constraint. We exemplified this by simulating the response of prosthetic vision to natural images
11 (Figure 6) using a convolutional linear-nonlinear (LN) model of RGCs^{40, 41}. After blurring the image by
12 convolution with the eye movement kernel (second column in Figure 6), we calculated the contrast
13 between the static component of the retinal image and the natural scene (Figure 6, third column).
14 Previously experimentally measured contrast sensitivity curves were used to convert the local
15 contrast into RGC firing rates (Figure 6, fourth column). With a complete characterization of the
16 spatial dependence of contrast sensitivity of prosthetic vision, this model could be expanded to take
17 into account the multiple spatial scales present in visual scenes and could lead to more accurate
18 predictions.

19 For simulation of normal vision, we used an image with the spatial resolution of the fovea (5 μ m pixel
20 pitch on the retina, Figure 6A). For simulation of prosthetic responses, images were first down-
21 sampled by the pixel size in order to reflect the expected spatial resolution of the implant¹¹.

22 Therefore, we used a 50 μ m and a 150 μ m square lattice sampling density and contrast sensitivity
23 curves as measured with the prosthesis (Figure 6 B and C). In the case of natural vision, this simple
24 model predicts strong responses localized, as expected, around the edges and textured areas.

25 However, in the case of prosthetic vision, it predicts an almost no responses due to its poor contrast
26 sensitivity to ON stimulation and lack of OFF responses.

27 **Discussion**

1 Bypassing the photoreceptors with subretinal electrical stimulation has strong implications on
2 contrast sensitivity and dynamic range of prosthetic vision. Light stimulation of the photoreceptors
3 leverages a finely tuned amplification cascade that can trigger responses to very dim illumination (a
4 few photons only, ^{42,43}), or to minute changes in contrast⁴⁴. Prosthetic subretinal stimulation of the
5 inner nuclear layer in the degenerate retina elicits responses with, at best, twice smaller amplitude
6 and ten times lower contrast sensitivity than normal.

7 While electrical stimulation of the healthy retina exhibits at least three types of responses to contrast
8 steps (eON, eOFF and eON-OFF), the eOFF component can be explained by electrical stimulation of
9 the photoreceptor layer. If only photoreceptors, bipolar and retinal ganglion cells were involved in
10 the response to full-field contrast steps, electrical stimulation of the photoreceptors should
11 depolarize them, thereby triggering action potentials and therefore apparent ON response in the OFF
12 pathway at the onset of electrical stimulation. When electrical stimulation stops, the photoreceptors
13 should hyperpolarize again, causing an electrical OFF response in the ON pathway this time. With
14 full-field stimulation of the rat retina, additional amacrine cell-mediated network effects further
15 complicate the response. This makes it difficult to pharmacologically dissect the mechanisms behind
16 the electrical OFF response. However, its progressive and almost complete disappearance with
17 advancing degeneration, correlated with disappearance of the photoreceptors in the RCS retina,
18 strongly indicates that it is indeed mediated by photoreceptors.

19 We did not observe a difference in contrast sensitivity between implants with 70 μ m and 140 μ m
20 pixels, indicative that while stimulation thresholds are affected by pixel size^{8,34}, the contrast
21 sensitivity function itself does not change once the retina adapts to above-threshold stimulation
22 levels at high frequency (>20Hz). The contrast sensitivity we measured matches values previously
23 observed in-vivo³⁴, and, importantly, it did not decline with age of the degenerate retinas (p90-140
24 vs. p300-400) despite the expected changes in the retinal network⁴⁵.

25 Subretinal stimulation preserves a few important features of retinal signal processing, such as flicker
26 fusion and transient responses to slower changes in luminance, as well as non-linear integration
27 across subunits of RGCs with large receptive fields¹¹. However, disappearance of the electrical OFF

1 responses means that both the ON and OFF pathways are activated simultaneously, a very unnatural
2 stimulation paradigm. Indiscriminate activation of all the cells in the inner nuclear layer is likely to
3 contribute to reduced contrast sensitivity since both excitatory bipolar and inhibitory amacrine cells
4 could be driven by the prosthesis. It remains unclear how this phenomenon affects phosphene
5 perception, since current clinical trials with subretinal prosthesis demonstrated that patients see
6 phosphenes primarily as light rather than dark flashes, and can perceive patterns of stimulation¹⁴.

7 The full-field measurements of contrast sensitivity we conducted do not take into account contrast
8 improvements at higher spatial frequencies due to center-surround effects in normal vision⁴⁶. It is
9 reasonable to expect this effect to be less pronounced with a subretinal prosthesis than with normal
10 vision since horizontal cells responsible for part of the center-surround effects in the retina are
11 thought to only synapse directly onto photoreceptors which disappear with degeneration, and not
12 bipolar cells⁴⁷. Therefore, only lateral inhibition from the amacrine cells should be able to contribute
13 to center-surround effects with subretinal prosthetic stimulation.

14 Contrast sensitivity of the system with patterned stimulation^{48, Loudin2007} is also strongly affected by
15 configuration of the return electrodes, and implants with distant returns exhibit significantly lower
16 electrical contrasts as compared to implants with local returns, such as those used in this study.

17 Making predictions about the human visual system based on measurements with a degenerate rat
18 retina is difficult, given the major differences between the visual systems of the two species. The
19 midget, parasol and small bistratified cells that dominate the human visual pathways⁴⁹ have no
20 anatomical equivalence in rat. It is possible that the magnocellular-projecting parasol cells would
21 have higher contrast sensitivities than the values we observed in rats. In addition, differences in the
22 rate and extent of retinal degeneration between humans and various animal models make it even
23 more difficult to predict responses to electrical stimulation in human patients.

24 An important consequence of the reduced contrast sensitivity and lack of OFF responses with
25 prosthetic vision is that efficiency of fixational eye movements for image refreshing and prevention
26 of perceptual fading^{13, 38} is greatly diminished, compared to natural vision. While it is possible to
27 deliver information with relatively high spatial content through the implant¹¹, most static visual

1 scenes are not sparse enough to elicit responses in RGCs with FEMs alone. This phenomenon could
2 be responsible for the perceptual fading at high stimulation frequencies reported in patients with the
3 subretinal implant Alpha-IMS, when FEMs which appear normal with the implant turned on⁵⁰ would
4 be expected to trigger retinal responses. Patients prefer stimulation frequencies not exceeding 7 Hz⁵⁰,
5 ⁵¹ – well below the flicker fusion frequency, so the pulses introduce strong temporal contrast in the
6 visual pattern. Lack of contrast sensitivity appears to be an important limitation of subretinal
7 prosthetic devices that can strongly impede their ability to deliver visual information efficiently to
8 the brain. This could be partially mitigated by pre-processing of the images between the camera and
9 the implant, which by increasing local image sparsity could bring local contrast above stimulation
10 thresholds.

11 **Acknowledgements**

12 We would like to thank Prof. E.J. Chichilnisky, M. Marmor, Drs. D. Boinagrov and H. Lorach for
13 stimulating discussions. We are grateful to Prof. A. Litke, P. Hottowy, S. Kachiguine and P. Hausser for
14 providing access to and support of the multielectrode array recording setup. We would like to thank
15 Dr. H. Lorach, R. Dalal and P. Huie for their help with histological images.

16

1 **Figures and tables**

2 Figure 1: **Stimulation protocol.** (A) With visible illumination, contrast steps are presented using
3 continuous illumination. (B) Prosthetic stimulation consists of contrast steps with the same envelope
4 modulating a 20Hz train of near-infrared pulses. (C), (D) Voltage traces from two different
5 electrodes. Note that the periodic “quiet” regions in these traces coincide with the removed
6 stimulation artifacts during which information about the waveform was lost due to amplifier
7 saturation. (C) Two neurons were detected on this electrode, one of which (larger amplitude action
8 potentials) responded transiently to the positive contrast step while the other (smaller action
9 potentials) did not respond to stimulation. (D) On this electrode, neurons transiently respond both to
10 the positive and the negative contrast steps.

11

12 Figure 2: **Single-unit responses to contrast steps.** (B) vON, (C) vON-OFF and (D) vOFF responses to (A)
13 full-field contrast steps observed with visible light in the WT retina. Neurons responded to both high
14 and low contrast steps. Similar (E) eON, (F) eON-OFF and weak (G) eOFF responses observed with
15 electrical stimulation in the degenerate RCS retina. With electrical stimulation, neurons did not
16 respond to lower contrast steps. The periodic gaps in the histograms are due to electrical stimulation
17 artifacts, which prevent detection of action potentials during the stimulation pulses.

18

19 Figure 3: **Histological analysis of the RCS rat retina.** (A) In the healthy WT retina, photoreceptor outer
20 segments (OS) transduce light and modulate the membrane potential of photoreceptor somas located
21 in the outer nuclear layer (ONL). Photoreceptors transmit neural information to cells in the inner
22 nuclear layer (INL), which then relay it to the ganglion cells (GCL). (B) In the P90 RCS retina, the
23 outer segments have been replaced by debris, and only a fraction of the photoreceptors somas
24 remain in the INL. (C) At P400, all the photoreceptor somas are gone from the RCS retina and only
25 the INL and GCL remain. Scale bar: 50µm.

26

1 Figure 4: **Mean population responses to contrast steps.** (A) WT responses to visible full field light steps
2 could broadly be classified into vON (red), vOFF (blue) and vON-OFF (purple) responses. The black
3 dashed line outlines the stimulation threshold, defined as a 50% probability of eliciting an action
4 potential correlated with the contrast step. On average, ON cells responded to contrast increments
5 greater than 7%, while OFF cells responded to contrast decrements as small as 3%. (B) Photovoltaic
6 stimulation of p90-140 RCS retina with 70 μ m pixel implants requires 67% contrast steps to elicit
7 responses in the RGCs. Maximum amplitude of the response is lower than with visible light in the WT
8 retina. Contrast sensitivity curves are very similar with (C) 140 μ m pixels used to stimulate p90-140
9 RCS retina and (D) in advanced stages of retinal degeneration (p300-400 RCS rats). Confidence band
10 represents the standard error of the mean.

11

12 Figure 5: **Effect of reduced contrast sensitivity on perception of 1-dimensional patterns.** The average
13 local luminance is estimated by convolving the light pattern (top row) with a blurring kernel defined
14 by the distribution of eye movements (middle row). The resulting local contrast is estimated and
15 compared to full-field contrast stimulation thresholds (bottom row). Red shaded area: above
16 threshold for prosthetic stimulation; blue shaded area: above threshold for visible light stimulation.
17 (A) In the case of a step, the local contrast between the image and the average local luminance is
18 below the threshold for infinitesimal eye movements (solid green line). Only large displacements of
19 the visual scene will result in a sufficiently large contrast between the average local luminance and
20 the visual scene to trigger responses (dashed green line, corresponding to a 90 μ m lateral
21 displacement also indicated on the blurring kernel). (B) In the case of a line, the pattern is sparse
22 enough to provide contrast exceeding stimulation threshold for both natural and prosthetic vision
23 even with small image displacements.

24

25 Figure 6: **Prosthetic response to a natural scene.** (A) Local contrast changes in a natural scene are large
26 enough to elicit robust RGC responses with normal vision. With prosthetic stimulation they are
27 insufficient to enable image refresh through microsaccades for implants with both (B) 50 μ m pixels
28 and (C) 150 μ m pixels.

1 **Tables**

2

	WT	RCS, p90-140	RCS, p300-400
eON	32%	68%	89%
eON-OFF	56%	30%	7%
eOFF	12%	2%	4%
Cell count	75	156	28

3

Table 1: Prevalence of eON, eOFF and eON-OFF responses in different animal models.

4

	OFF-center	ON-center
eON	56%	14%
eON-OFF	22%	83%
eOFF	22%	3%

5

Table 2: Mapping visible light responses to prosthetic responses.

6

7

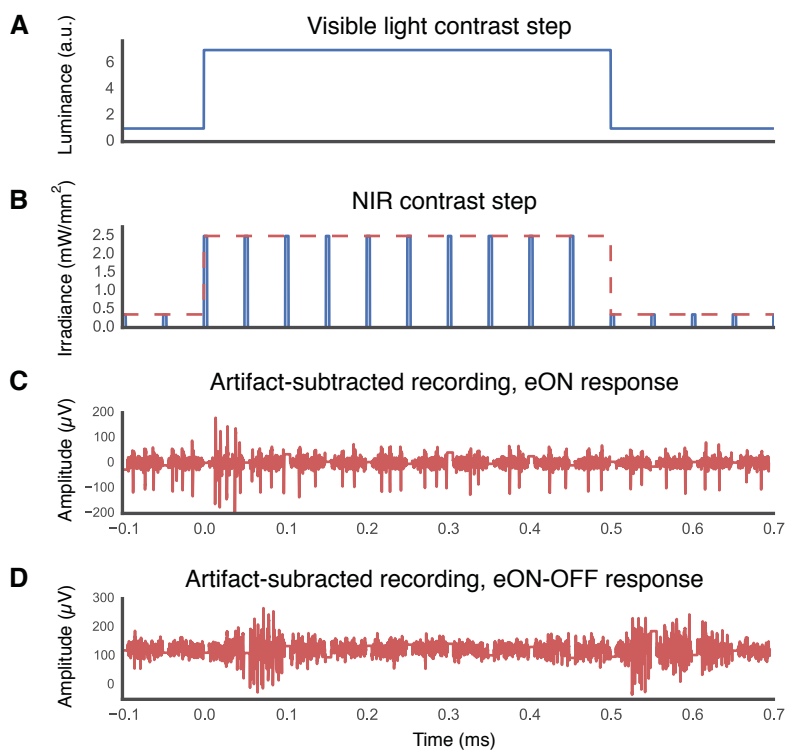
References

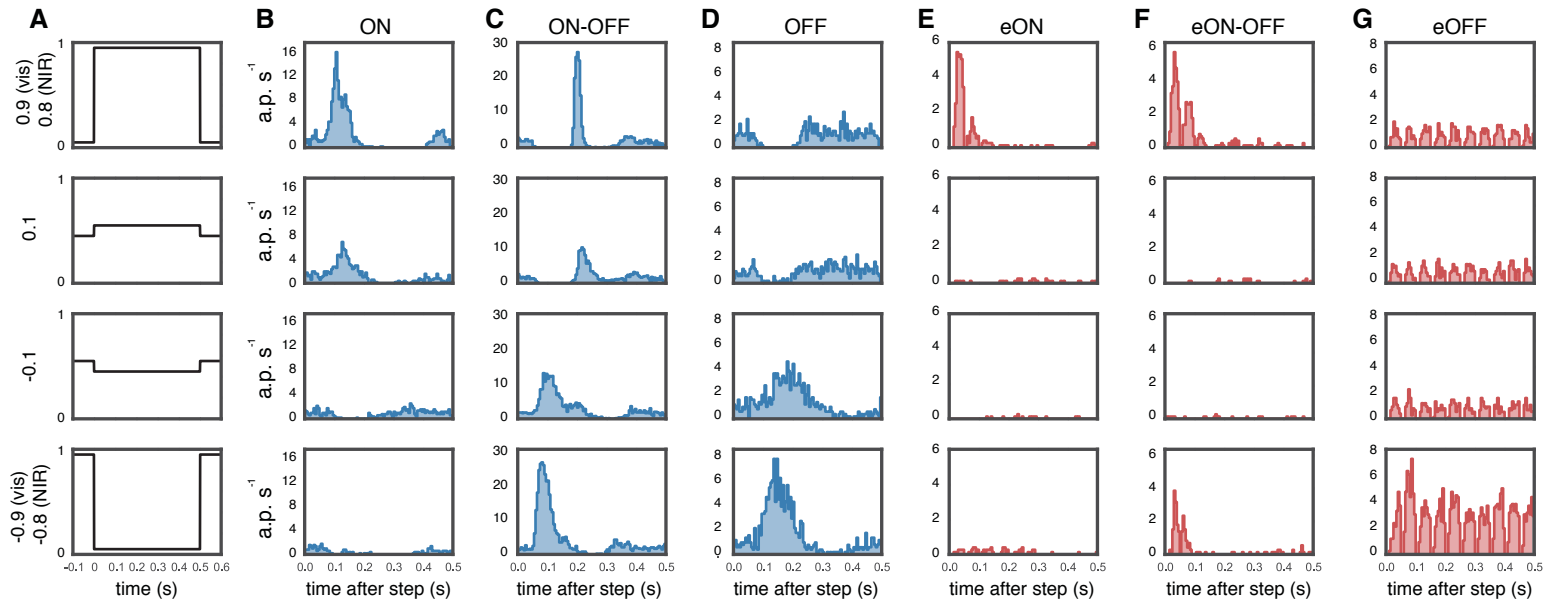
- 1
2
3 1. Smith W, Assink J, Klein R, et al. Risk factors for age-related macular
4 degeneration: Pooled findings from three continents. *Ophthalmology*
5 2001;108:697-704.
- 6 2. Mazzoni F, Novelli E, Strettoi E. Retinal ganglion cells survive and maintain
7 normal dendritic morphology in a mouse model of inherited photoreceptor
8 degeneration. *J Neurosci* 2008;28:14282-14292.
- 9 3. Humayun MS, Prince M, de Juan E, et al. Morphometric analysis of the
10 extramacular retina from postmortem eyes with retinitis pigmentosa. *Invest*
11 *Ophthalmol Vis Sci* 1999;40:143-148.
- 12 4. Kim SY, Sadda S, Pearlman J, et al. Morphometric analysis of the macula in eyes
13 with disciform age-related macular degeneration. *Retina* 2002;22:471-477.
- 14 5. Marc RE, Jones BW. Retinal Remodeling in Inherited Photoreceptor
15 Degenerations. *Molecular Neurobiology* 2003;28:139-147.
- 16 6. Jensen RJ, Rizzo JF. Thresholds for activation of rabbit retinal ganglion cells
17 with a subretinal electrode. *Experimental eye research* 2006;83:367-373.
- 18 7. Mathieson K, Loudin J, Goetz G, et al. Photovoltaic Retinal Prosthesis with High
19 Pixel Density. *Nat Photonics* 2012;6:391-397.
- 20 8. Mandel Y, Goetz G, Lavinsky D, et al. Cortical responses elicited by photovoltaic
21 subretinal prostheses exhibit similarities to visually evoked potentials. *Nat*
22 *Commun* 2013;4:1980.
- 23 9. Goetz GA, Mandel Y, Manivanh R, Palanker DV, Cizmar T. Holographic display
24 system for restoration of sight to the blind. *Journal of neural engineering*
25 2013;10:056021.
- 26 10. Boinagrov D, Lei X, Goetz G, et al. Photovoltaic Pixels for Neural Stimulation:
27 Circuit Models and Performance. *IEEE Trans Biomed Circuits Syst* 2015.
- 28 11. Lorach H, Goetz G, Smith R, et al. Photovoltaic restoration of sight with high
29 visual acuity. *Nature Medicine* 2015;in print.
- 30 12. Kuang X, Poletti M, Victor JD, Rucci M. Temporal encoding of spatial
31 information during active visual fixation. *Curr Biol* 2012;22:510-514.
- 32 13. Rucci M, Victor JD. The unsteady eye: an information-processing stage, not a
33 bug. *Trends Neurosci* 2015;38:195-206.
- 34 14. Stingl K, Bartz-Schmidt K-U, Gekeler F, Kusnyerik A, Sachs H, Zrenner E.
35 Functional Outcome in Subretinal Electronic Implants Depends on Foveal
36 Eccentricity. *Investigative Ophthalmology & Visual Science* 2013;54:7658-7665.
- 37 15. Wang L, Mathieson K, Kamins TI, et al. Photovoltaic retinal prosthesis: implant
38 fabrication and performance. *Journal of neural engineering* 2012;9:046014.
- 39 16. Litke AM, Bezayiff N, Chichilnisky EJ, et al. What Does the Eye Tell the Brain?
40 Development of a System for the Large-Scale Recording of Retinal Output
41 Activity. *IEEE Trans on Nuclear Science* 2004;51:1434-1440.
- 42 17. Whitley E, Ball J. Statistics review 4: Sample size calculations. *Crit Care*
43 2002;6:335-341.
- 44 18. Chichilnisky EJ. A simple white noise analysis of neuronal light responses.
45 *Network: Comput Neural Syst* 2001;12:199-213.

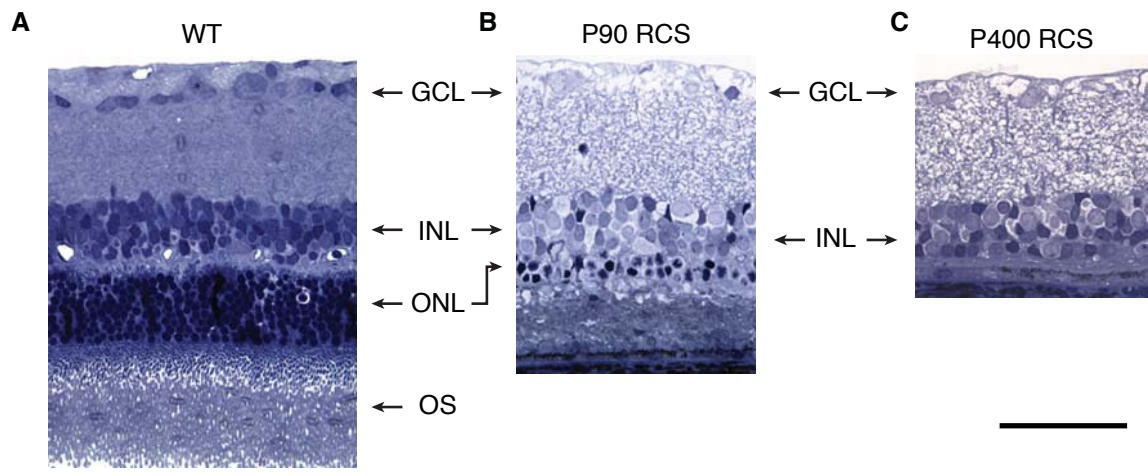
- 1 19. Chichilnisky EJ, Kalmar RS. Functional Asymmetries in ON and OFF Ganglion
2 Cells of Primate Retina. *The Journal of Neuroscience* 2002;22:2737-2747.
- 3 20. Boinagrov D, Pangratz-Fuehrer S, Goetz G, Palanker D. Selectivity of Direct and
4 Network-mediated Stimulation of the Retinal Ganglion Cells with Epi-, Sub-
5 and Intra-Retinal Electrodes. *Journal of neural engineering* 2014;11:026008.
- 6 21. Lewicki MS. A review of methods for spike sorting: the detection and
7 classification of neural action potentials. *Network: Comput Neural Syst*
8 1998;9:R53-R78.
- 9 22. Petrusca D, Grivich MI, Sher A, et al. Identification and characterization of a Y-
10 like primate retinal ganglion cell type. *The Journal of neuroscience : the official*
11 *journal of the Society for Neuroscience* 2007;27:11019-11027.
- 12 23. Greschner M, Field GD, Li PH, et al. A polyaxonal amacrine cell population in
13 the primate retina. *The Journal of neuroscience : the official journal of the*
14 *Society for Neuroscience* 2014;34:3597-3606.
- 15 24. Li PH, Gauthier JL, Schiff ML, et al. Anatomical Identification of Extracellularly
16 Recorded Cells in Large-Scale Multielectrode Recordings. *J Neurosci*
17 2015;31:xxxx-xxxx.
- 18 25. Devries SH, Baylor DA. Mosaic Arrangement of Ganglion Cell Receptive Fields
19 in Rabbit Retina. *Journal of neurophysiology* 1997;78:2048-2060.
- 20 26. Field GD, Sher A, Gauthier JL, et al. Spatial properties and functional
21 organization of small bistratified ganglion cells in primate retina. *The Journal of*
22 *neuroscience : the official journal of the Society for Neuroscience*
23 2007;27:13261-13272.
- 24 27. Dacey DM, Petersen MR. Dendritic field size and morphology of midget and
25 parasol cells of the human retina. *PNAS* 1992;89:9666-9670.
- 26 28. Wassle H. Parallel processing in the mammalian retina. *Nat Rev Neurosci*
27 2004;5:747-757.
- 28 29. Heine WF, Passaglia CL. Spatial receptive field properties of rat retinal ganglion
29 cells. *Visual Neuroscience* 2011;28:403-417.
- 30 30. Borst A, Euler T. Seeing things in motion: models, circuits, and mechanisms.
31 *Neuron* 2011;71:974-994.
- 32 31. Olveczky BP, Baccus S, Meister M. Segregation of object and background
33 motion in the retina. *Nature* 2003;423:401-408.
- 34 32. Sekirnjak C, Hottowy P, Sher A, Dabrowski W, Litke AM, Chichilnisky EJ.
35 Electrical stimulation of mammalian retinal ganglion cells with multielectrode
36 arrays. *Journal of neurophysiology* 2006;95:3311-3327.
- 37 33. Jepson LH, Hottowy P, Mathieson K, et al. Focal electrical stimulation of major
38 ganglion cell types in the primate retina for the design of visual prostheses. *The*
39 *Journal of neuroscience : the official journal of the Society for Neuroscience*
40 2013;33:7194-7205.
- 41 34. Lorach H, Goetz G, Mandel Y, et al. Performance of photovoltaic arrays in-vivo
42 and characteristics of prosthetic vision in animals with retinal degeneration.
43 *Vision Res* 2014.
- 44 35. Shapley RM, Enroth-Cugell C. Visual Adaptation and Retinal Gain Controls. In:
45 Osborne N, Chader G (eds), *Progress in Retinal Research*. Oxford; 1984:263-
46 346.

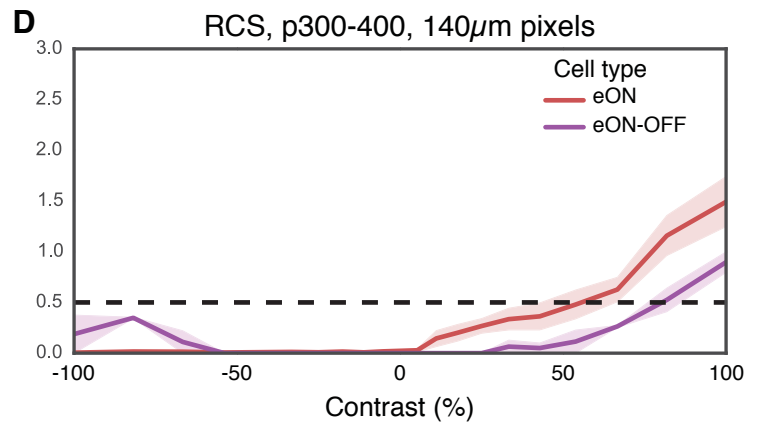
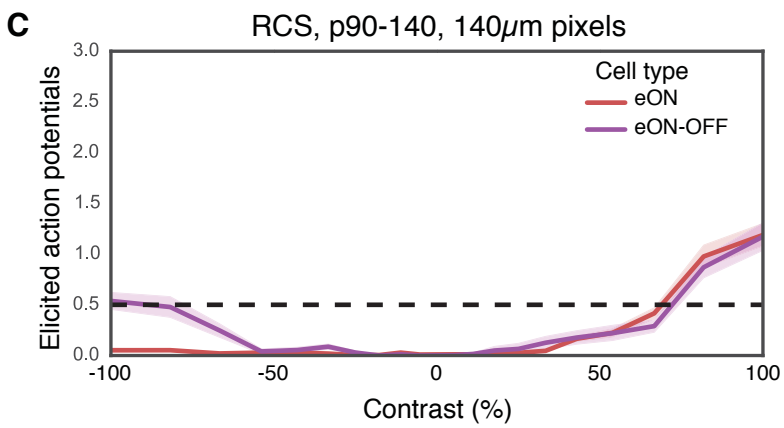
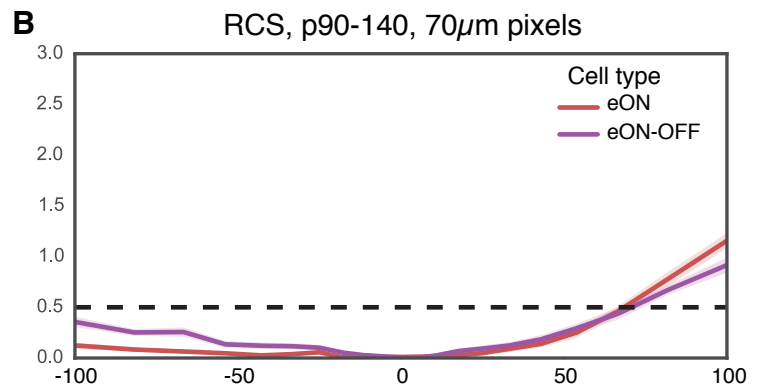
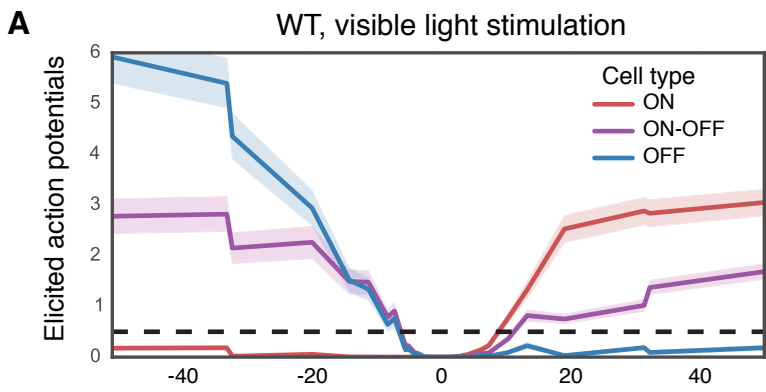
- 1 36. Shapley RM, Kaplan E, Purpura KP. Contrast Sensitivity and Light Adaptation in
2 Photoreceptors or in the Retinal Network. In: Shapley RM, Lam DM-K (eds),
3 *Contrast sensitivity*: M.I.T. Press; 1993:103-116.
- 4 37. Shapley RM. Retinal physiology: Adapting to the changing scene. *Current*
5 *Biology* 1997;7:R412-R423.
- 6 38. McCamy MB, Otero-Millan J, Macknik SL, et al. Microsaccadic efficacy and
7 contribution to foveal and peripheral vision. *The Journal of neuroscience : the*
8 *official journal of the Society for Neuroscience* 2012;32:9194-9204.
- 9 39. Martinez-Conde S, Macknik SL, Troncoso XG, Hubel DH. Microsaccades: a
10 neurophysiological analysis. *Trends in Neurosciences* 2009;32:463-475.
- 11 40. Paninski L. Maximum likelihood estimation of cascade point-process neural
12 encoding models. *Network: Computation in Neural Systems* 2004;15:243-262.
- 13 41. Truccolo W, Eden UT, Fellows MR, Donoghue JP, Brown EN. A point process
14 framework for relating neural spiking activity to spiking history, neural
15 ensemble, and extrinsic covariate effects. *Journal of neurophysiology*
16 2005;93:1074-1089.
- 17 42. Baylor DA, Lamb TD, Yau K-W. The Membrane Current Of Single Rod Outer
18 Segments. *J Physiol* 1979;288:589-611.
- 19 43. Rieke F, Baylor DA. Single-photon detection by rod cells of the retina. *Reviews*
20 *of Modern Physics* 1998;70:1027-1036.
- 21 44. van Alphen B, Winkelman BH, Frens MA. Age- and sex-related differences in
22 contrast sensitivity in C57BL/6 mice. *Invest Ophthalmol Vis Sci* 2009;50:2451-
23 2458.
- 24 45. Marc RE, Jones BW, Watt CB, Strettoi E. Neural remodeling in retinal
25 degeneration. *Progress in Retinal and Eye Research* 2003;22:607-655.
- 26 46. Derrington AM, Lennie P. Spatial and Temporal Contrast Sensitivities of
27 Neurones in Lateral Geniculate Nucleus of Macaque *J Physiol* 1984;357:219-
28 240.
- 29 47. Kolb H, Mariani A, Gallego A. A second type of horizontal cell in the monkey
30 retina. *J Comp Neurol* 1980;189:31-44.
- 31 48. Palanker D, Vankov A, Huie P, Baccus S. Design of a high-resolution
32 optoelectronic retinal prosthesis. *J Neural Eng* 2005;2:S105-120.
- 33 49. Dacey DM. Origins of perception: retinal ganglion cell diversity and the
34 creation of parallel visual pathways. In: Gazzaniga MS (ed), *The Cognitive*
35 *Neurosciences*: MIT Press; 2004:281-301.
- 36 50. Hafed ZM, Stingl K, Bartz-Schmidt K U, Gekeler F, Zrenner E. Oculomotor
37 behavior of blind patients seeing with a subretinal visual implant. *Vision Res*
38 2015;in press.
- 39 51. Stingl K, Bartz-Schmidt KU, Besch D, et al. Artificial vision with wirelessly
40 powered subretinal electronic implant alpha-IMS. *Proceedings Biological*
41 *sciences / The Royal Society* 2013;280:20130077.

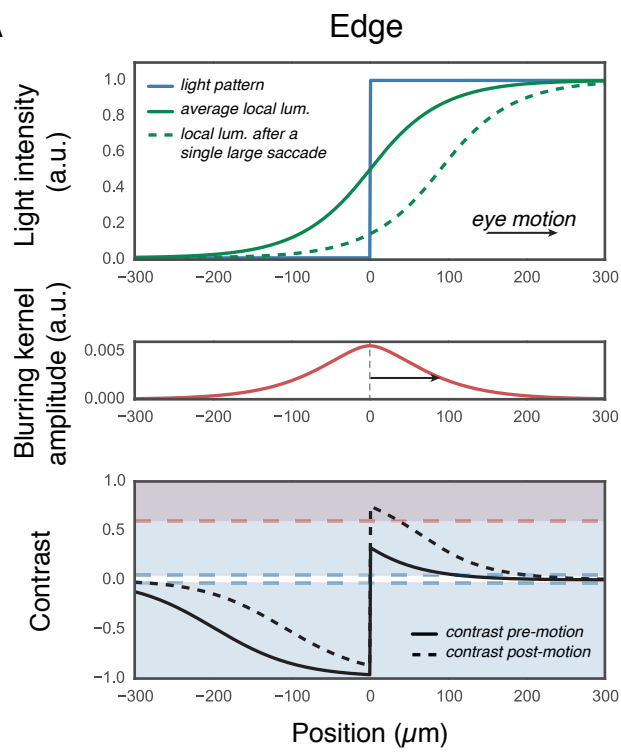
42
43









A**B**